UCRL_____

UNIVERSITY OF CALIFORNIA

Radiation Laboratory

BERKELEY, CALIFORNIA

UCRL-2799
Unclassified Physics

UNIVERSITY OF CALIFORNIA
Radiation Laboratory
Berkeley, California

Contract No. W-7405-eng-48

NEGATIVE PIONS FROM NEUTRON BOMBARDMENT OF DEUTERONS

Myron William Knapp
(Thesis)

November, 1954

Printed for the U.S. Atomic Energy Commission

NEGATIVE PIONS FROM NEUTRON BOMBARDMENT OF DEUTERONS

Contents

NEGATIVE PIONS FROM NEUTRON BOMBARDMENT OF DEUTERONS

Myron William Knapp

Radiation Laboratory, Department of Physics
University of California, Berkeley, California

November, 1954

ABSTRACT

In order to obtain information on the neutron-neutron interaction, a cloud chamber filled with deuterium gas was bombarded with the neutron beam of the Berkeley 184-inch synchrocyclotron. The spectrum of the neutron beam, which is produced by 340-Mev protons on a 2-1/2-inch lithium deuteride target, is peaked at 300 Mev and extends to 340 Mev. The three reactions $d(n,\pi^- p)d$, $d(n,\pi^- pn)p$, and $d(n,\pi^-)He^3$ were studied. A total of 310 events were examined; the three reactions contributed 208, 80, and 22 events respectively. Laboratory-system angular distributions and energy spectra of the mesons are presented.

NEGATIVE PIONS FROM NEUTRON BOMBARDMENT OF DEUTERONS

Myron Williams Knapp

Radiation Laboratory, Department of Physics
University of California, Berkeley, California

November, 1954

INTRODUCTION

Many of the recent experiments[1, 2, 3] on meson physics have sought information on charge symmetry and charge independence of nuclear forces. The latter hypothesis, as formulated in the principle of conservation of isotopic spin, permits all cross sections for pion production in nucleon-nucleon collisions to be written in terms of three independent cross sections,[4] whereas the weaker principle of conservation of isotopic parity relates only the neutron-neutron interactions to the proton-proton ones. Either of these hypothesis predicts that the cross section for the reaction $p + p \rightarrow \pi^+ + d$ will be the same as that for the reaction $n + n \rightarrow \pi^- + d$. This is also true for the angular distributions in both reactions. Because the latter reaction cannot be observed directly, the reaction $n + d \rightarrow \pi^- + 3$ nucleons has been substituted. An exact knowledge of the condition of the neutron in the deuteron when it is struck by the incoming neutron should permit the calculation of the angular distribution of the pions in the center-of-mass system of the two neutrons. Ideally one would compare this distribution with the $(1/3 + \cos^2 \theta)$ obtained for π^o mesons by neutrons on protons[5, 6, 7] and for π^o mesons by neutrons on protons.[1] The unknown momentum of the neutron in the deuteron, however, makes a transformation to the center-of-mass system of the two neutrons impossible. Therefore the alternative possibility was chosen, and laboratory-system distributions are presented for comparison with theoretical distributions as derived from the known neutron spectrum and known momentum wave functions of the deuteron. Owing to difficulties in monitoring the high-energy portion of the neutron beam, no attempt was made to determine absolute cross sections, and the results are presented in terms of relative angular distributions and energy spectra for the three reactions involved.

A cloud chamber seemed the most feasible detector of negative pion

production for the following three reactions:

(a) The three possible reactions

$$n + d \rightarrow \pi^- + p + d,$$
$$n + d \rightarrow \pi^- + 2p + n,$$
$$n + d \rightarrow \pi^- + He^3.$$

could be individually identified, and a ratio of their production frequency thus obtained.

(b) Mesons at all angles and energies could be examined simultaneously.

(c) The three- and four-body problems involved would make a counter experiment impractical.

One of the great disadvantages in using a cloud chamber in this experiment is a low data rate. (It took on the average, thirty minutes of cyclotron time to obtain each event.) Two factors, other than the small cross section, limit the data rate. They are a relatively long cycle time (about two minutes), and a certain maximum amount of beam per cycle, this being limited by the large background from the low-energy tail of the neutron beam. Both these factors have been pushed to their limits, so that the pictures are very crowded, and occasionally high-energy tracks fade near the top glass. For this reason, the pictures were not always of the best quality. In order to be confident that certain types of events were not lost because of picture quality, several symmetry distributions were made. These are recorded in the chapter on Experimental Checks and Discussion of Errors.

The reactions leading to production of positive and neutral-pions in neutron-deuteron collisions are also of interest, but unfortunately impractical to study with a cloud chamber. In a π^+ event, for example, the cloud chamber would show only the π^+ meson, which would be very difficult to find in the heavy background of other positive particles. Occasionally one was discovered, but it is unreasonable to assume that any significant fraction was seen. As suggested by several authors[8,9] a comparison of the $n + d \rightarrow \pi^- + He^3$ reaction with $n + d \rightarrow \pi^o + He^3$ would yield important information about charge independence. This is the only one of the three possible π^o reactions that might be identified in a cloud chamber; although the triton could be identified from its momentum and

and relative ionization, the deuteron or proton produced if the triton were split up would not look different from a neuteron or proton scattered by a low-energy neutron. In order to identify the tritons with certainty, however, the pictures would have to be good quality, and some sacrifice would have to be made in the data rate. Since one would expect half as many π^o triton events as π^- He^3 events, and since only 22 He^3 events were obtained during the course of the experiment, it would be impractical to attempt this investigation with a cloud chamber.

EXPERIMENTAL PROCEDURE

Apparatus

Cloud Chamber

One of the vital parts of the experimental apparatus was a ten-atmosphere Wilson cloud chamber, designed and built at this laboratory by Dr. John De Pangher, Jr. His paper[10] gives a very thorough discussion of the cloud chamber, and only a brief description of it need be given here.

The sensitive volume of the chamber is a cylinder about 10 inches in diameter and 2.5 inches in height. This cylinder is bounded by a 1.25-inch-thick top glass, a 0.75 inch-thick lucite cylinder 12 inches in diameter, and a rubber diaphragm mounted on a 0.5-inch-thick lucite piston. Pantograph arms restrain the piston in such a way that it is at all times parallel to the top glass. A layer of black gelatin on the piston serves as a source of water vapor, provides a photographic background, and acts as one of the clearing field surfaces. The other clearing field surface is supplied by a soap film and an aquadag ring on the top glass.

Photography

Photographs are taken by a specially designed stereoscopic camera using Leica Summitar 50-mm lenses and 1.8-inch Kodak Linograph Pan film. Light for the photography is supplied through the lucite cylinder of the cloud chamber by two General Electric F. T. 422 flash tubes. A 250-microfarad bank of condensers, charged to 1,700 volts, is discharged through each of the flash tubes; the length of this light flash, about 100 microseconds, determines the length of the exposure (the camera has no shutter).

An automatic developer attached directly to the camera made it possible to examine pictures about 15 minutes after they were taken. This permitted a continuous check on operating conditions.

Neutron Beam

The neutron beam was produced by bombarding a 2.5 inch-thick lithium deuteride target with 340-Mev protons in the 184-inch synchrocyclotron. Figure 1 show the preliminary collimation in the igloo and

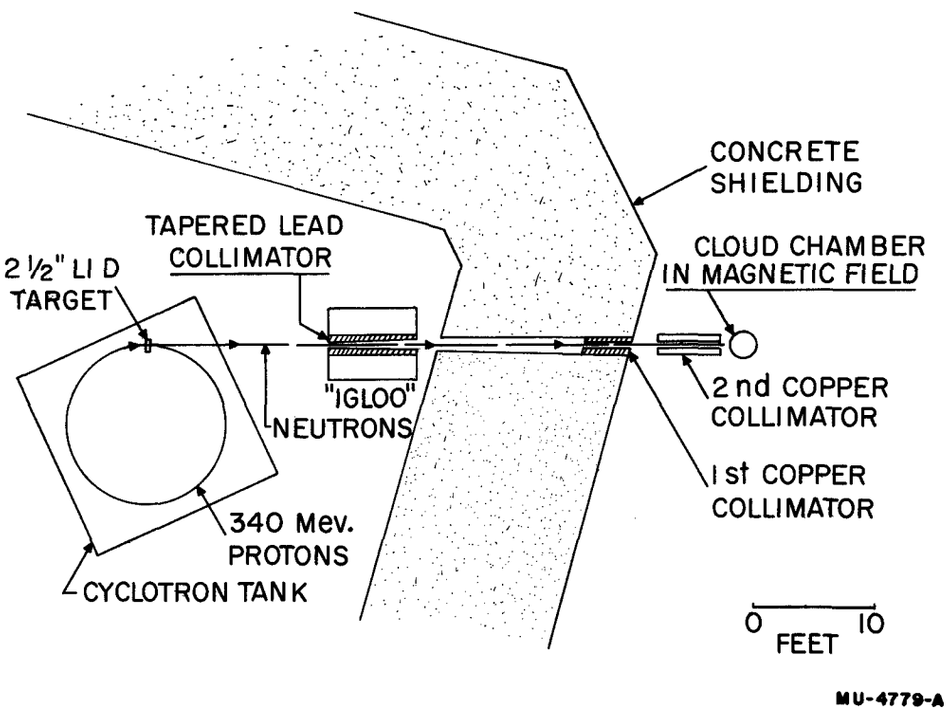

Fig. 1 The collimating system.

the neutron port, as well as the 3-ft copper collimator immediately in front of the cloud chamber The preliminary collimator served only to reduce background from the final collimator, which reduced the beam to the desired size of 2 1/4 x 5/8 inches.

Magnetic Field

The necessary magnetic field was produced by pulsing a 150-hp mine-sweeper generator through the coils of the cloud chamber magnet. When pulsed, this generator supplies 4,000 amp to the magnet, producing a field of 21,7000 gauss. This field is uniform to within 2.5% over the usable region of the cloud chamber, and the field at the center of a track is obtained from a uniformity plot.

Temperature Control

The temperature of the cloud chamber is controlled by circulating water at 20°C through heat shields surrounding the cloud chamber and through water jackets at various places on the cloud chamber itself.

Sequence of Operation

To allow time after each expansion for resupplying water vapor near the top glass, a two-minute cycle was necessary.* The sequence of events during a cycle was as follows:

1. Magnet energized
   It takes 2.5 seconds for the field to reach its peak value, where it stays for about 0.15 seconds.
2. Clearing field off
3. Fast expansion
   This is timed so that the field reaches its peak just as the piston hits bottom.
4. Cyclotron pulsed
   The first of four or five cyclotron pulses coincides in time with piston's hitting bottom.
5. Lights flashed
   The lights are flashed about 0.1 second after the last beam pulse.
6. Clearing field on
7. Two slow expansions
   These expansions clear out old center of condensation.

* A longer cycle would have produced better pictures but a lower data rate.

8. Repeat cycle
   One and a half minutes are allowed after the second slow expansion for re-establishment of the required conditions.

Analysis of Film

Description of an Event and Sample Pictures

Three types of events are possible in this experiment, and scanning procedure is determined by their appearance. Table I shows the three types together with

Table I

Event	Type	Q(Mev)
$n + d \rightarrow \pi^- + p + d$	d	138
$n + d \rightarrow \pi + 2p + n$	p	140
$n + d \rightarrow \pi^- + He^3$	He^3	133

their Q values. The first is referred to as a 'd' or deuteron type, the second as a 'p' or proton type, and the third as a He^3 type event.

Because there is no unseen particle in either the d or He^3 type events they must show a total forward momentum equal to that of the incident neutron, and transverse momentum must balance. The p type event has an unseen neutron, therefore particles that are seen need not have as much total forward momentum as the other two types, and their transverse momentum need not balance. It also follows from momentum considerations that the pion, being light, can have any direction relative to the neutron beam and that the proton in a d-type or one of the protons in a p-type event can come off in a backwards direction, if its energy is fairly low.

An event consists, therefore of one lightly ionized track of nagative curvature and one or two positive tracks with considerable forward mo-

mentum. Figures 2, 3, 4, and 5 are pictures of typical events. In Fig. 2 is seen a 152-Mev forward deuteron, a dot at the origin caused by a proton of less than 0.5 Mev and a 21-Mev pion. The heavy forward track in Fig. 3 is a 69-Mev He^3. The pion in this picture has 73 Mev. Figure 4 was included because it was the only event in which the pion stopped and produced a visible star. In this picture the pion has 1 Mev, one proton has 100 Mev, and the other proton 4 Mev. Figure 5 has two easily visible π^- events and one π^+ event. The π^+ shows how difficult it is to spot π^+ mesons in this experiment.

Scanning Procedure and Methods

Two scanning methods were used. One of these employed a stereoscopic viewer, of a high magnifying power, through which one could examine track origins, looking for more than one track starting at the same point in space. In this manner oxygen stars from the oxygen in the water vapor, pion events of the three types mentioned above, and two-prong stars were found. The two-prong stars could be fitted into one of three categories; they could either be oxygen stars, or coincidences, or pion events in which the meson was hidden or unseen for some reason. Therefore all two-prong stars had to be examined in detail to be sure that no pion events were missed, and those for which no explanation was apparent are discussed in a later section.

Also noted during scanning were any negative mesons that appeared to start in the collimated region but for which no associated tracks were apparent. These were examined more thoroughly on the projection apparatus, and in all but one case the meson was either traced back to an event or to a point outside the illuminated region.

The second scanning method involved projecting the cloud chamber pictures to approximately twice normal size and examining one of the paired stereoscopic views at a time for tracks starting at the same point. By quickly shifting from one stereoscopic view to the other, one could decide whether or not tracks started at the same point in space. The procedure in other respects was the same as above. Only about 1/4 of the pictures were scanned in this manner, but the fraction of events missed in the one scanning was the same as that in the other method.

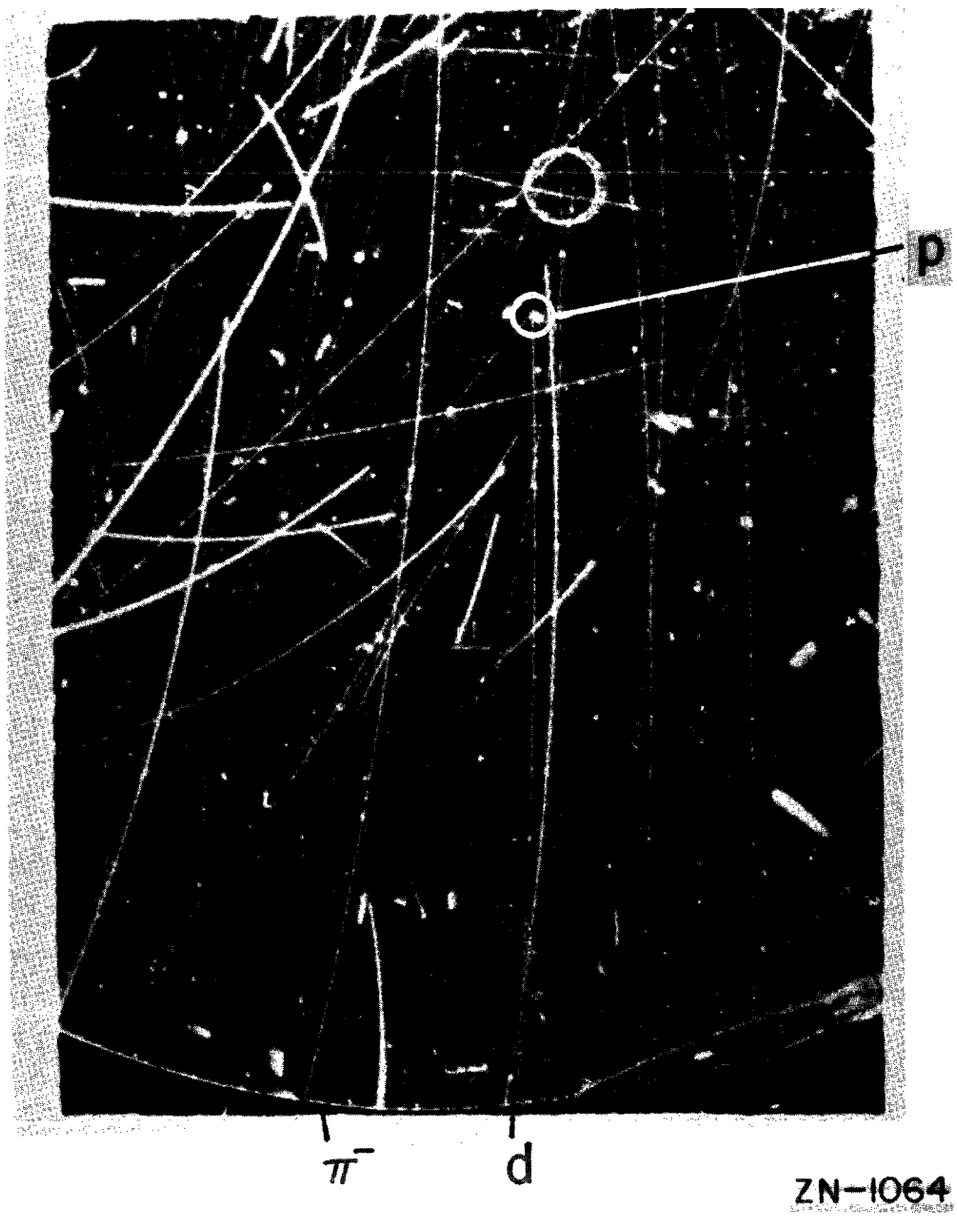

Fig. 2 Cloud chamber picture. An example of the reaction $n + d \rightarrow \pi^- + p + d$. The origin of the event is encircled.

Fig. 3 Cloud chamber picture. The circle surrounds the origin of an event of the type $n + d \rightarrow \pi^- + He^3$.

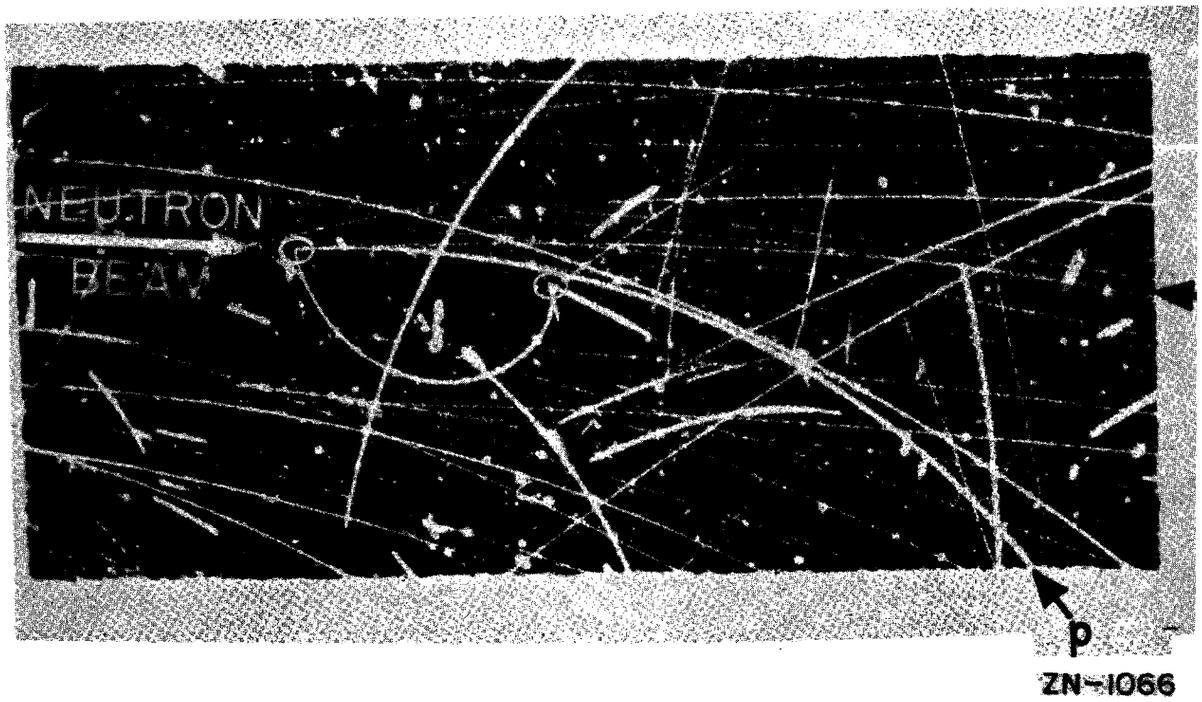

Fig. 4 Cloud chamber picture. One circle in this picture surrounds the origin of an event of the type $n + d \rightarrow \pi^- + 2p + n$ and the other surrounds the point where the π^- stops. The π^- is captured at this point by an oxygen nucleus which it explodes into three visible fragments.

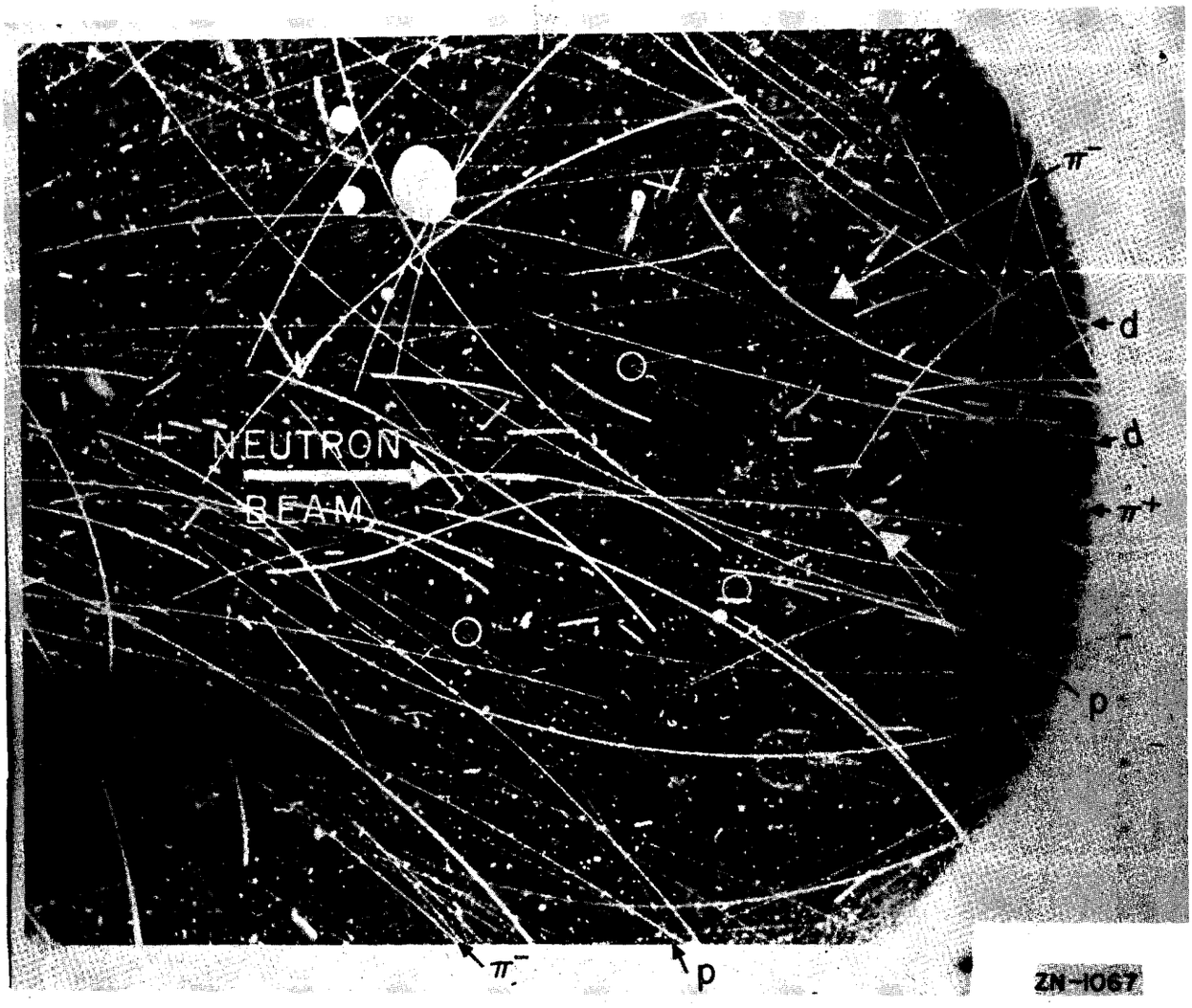

Fig. 5 Cloud chamber picture. This picture contains three events, two of the type $n + d \rightarrow \pi^- + p + d$ and one of the type $n + d \rightarrow \pi^+ + 3n$. The three origins are encircled.

Measurement Procedure

Those pictures containing events were projected according to the method used by previous cloud chamber experimenters,[10-13] onto a translucent screen by means of the stereoscopic projection apparatus shown schematically in Fig. 6. The translucent screen on which the images were focused has three degrees of translatory motion and two degrees of rotational freedom. By proper adjustment of the position of this translucent screen, the two stereoscopic images of a given track could be brought into coincidence. When this was accomplished the original direction and position of the track in space was reproduced. The quantities determined for every track, together with the definitions of these quantities are listed in Table II.

These data were recorded on Keysort Cards,* one track per card. The film number and trace number provided a means of identifying the two or three cards belonging to a single event.

Analysis of the Data

Calculations Pertaining to Each Track

The quantities calculated for each track, together with the definitions of the quantities and the formulas used in their calculation, are listed in Table III. The formulas listed in Table III have been used or derived in previous cloud chamber experiments,[10-13] and their derivations are not presented here. Figures 22 and 23 of Appendix I give $B\rho$ vs T for pions and protons respectively. If both scales of Fig. 23 are multiplied by 2, Fig. 23 then gives $B\rho$ vs T for deuterons. This follows because a deuteron, having twice the momentum of a proton, has twice the energy of that proton. A similar function scale was used for the He^3, but was not prepared for publication.

---

* Keysort Cards provided a rapid and convenient form for analyzing data.

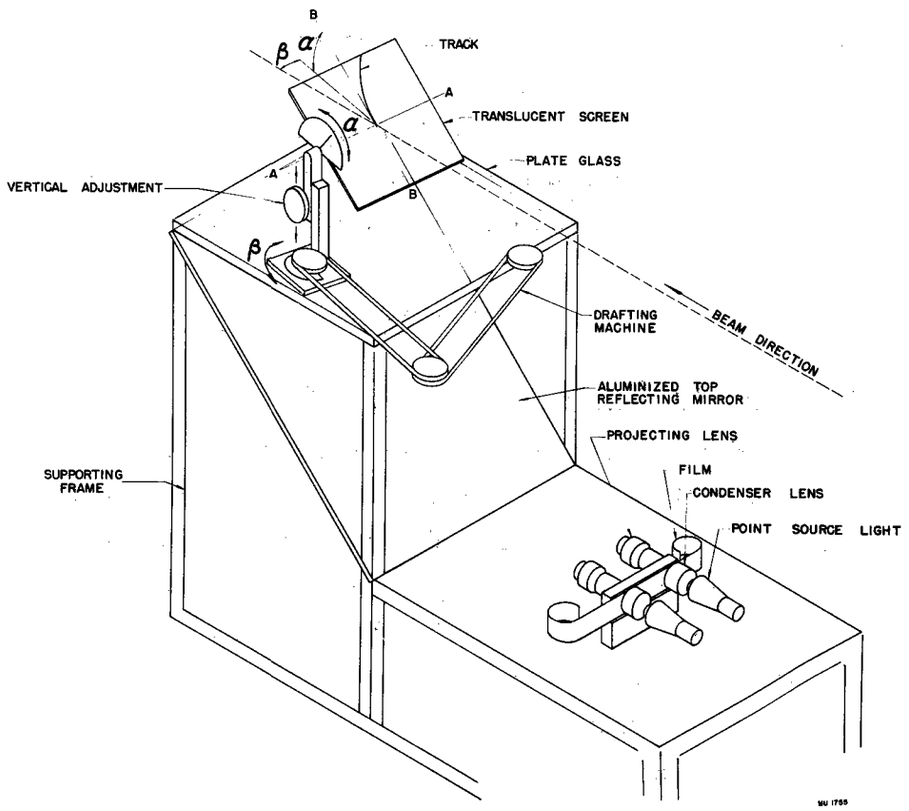

Fig. 6 The stereocopic projection apparatus.

Table II

Quantities Determined for Each Track

Dip Angle α	The angle between the horizontal plane* and the osculating plane** of the track.
Beam Angle β	The angle between the neutron beam and a vertical plane through the initial track direction.
Radius ρ***	The radius of curvature of the track as measured in its osculating plane.**
Range R***	The length of the track if the particle stops in the gas.
Length L	The length of a track over which ρ is measured.
Height z_o	The height of the origin of the track.
Height z_m	The height of the middle of the track.
Distance r	The distance from the middle of the track to the center of the chamber.
Temporary Identification	The tentative identification of each track as that of a π, p, d, or He^3, based on relative ionization.
Film Number	The number of the stereoscopic pair of pictures in which the event was recorded.
Trace Number	The number of each track, for identification purposes, as defined in a tracing of the event.

---

* The neutron beam lies in the horizontal plane.

** The tracks of course are actually segments of a helix, but the length over which they are measured, for a given radius, is sufficiently small to assume that they lie in a plane, which we call the osculating plane.

*** If the particle stops in the gas, the range is determined instead of the radius.

Table III

Quantities Calculated for Each Track

B	$B = B(z_m, r)$ From a table.	Magnetic field strength at middle of track (in gauss)
p	$p = B\rho \cos \alpha$*	Momentum of particle (in gauss-cm
T	$p = \frac{10^4}{3}\sqrt{T^2 + 2Mc^2T}$**	The kinetic energy of the particle (in Mev)
θ	$\cos \theta = \cos \alpha \cos \beta$	The scatter angle, i.e. the angle between the initial track direction and the neutron beam.
p_x	$p_x = p \cos \alpha \cos \beta$	Longitudinal momentum component, i.e. the momentum component along the beam direction.
p_y	$p_y = p \cos \alpha \sin \beta$	Horizontal transverse momentum component
p_z	$p_z = p \sin \alpha$	Vertical transverse momentum component
$f(\theta, \alpha_o)$	$f(\theta, \alpha_o) = \frac{\pi/2}{\sin^{-1}\left(\frac{\sin \alpha_o}{\sin \theta}\right)}$	Geometric correction factor (see section on Dip Angle Limitations)
ϕ	$\tan \phi = \tan \alpha \csc \beta$	The azimuthal angle, i.e. the angle between the horizontal plane and a plane containing both the neutron beam and the initial track direction.

* In the case of a He^3 p equals $2B\rho \cos \alpha$.

** In the case of a range measurement T is obtained from the range-energy relations in Appendix I, Fig. 24.

Calculations Pertaining to Each Event

Although Tables II and III contain all data pertinent to a given track, calculations on the event as a whole yield important information as to the final identification of each particle and the energy of the neutron causing the event. The quantities used in these calculations are defined in Table IV.

Table IV

$\sum_j p_{xj}$, $\sum_j p_{yi}$, $\sum_j p_{zj}$	The sums, respectively, of the longitudinal and the horizontal and vertical transverse momentum components over all tracks of the event.
$T_n(p)$	The kinetic energy of a neutron whose momentum is p.
$\sum_j T_j$	The sum of the kinetic energies over all tracks of the event.
T_n	The energy of the incident neutron
T_n', p_n', $p_{n'x}$, $p_{n'y}$, $p_{n'z}$	The energy, momentum, and momentum components of the outgoing neutron in a p-type event.
Q	The Q value of the reaction as given in Table I.

In either a d- or H_e^3-type event, these definitions, together with the laws of conservation of energy and momentum, lead to the following equations:

$$T_n = T_n\left(\sum_j p_{xj}\right) = \sum_j T_j + Q$$

$$\sum_j p_{yj} = 0$$

$$\sum_j p_{zj} = 0$$

These equations provide a positive check on the identification of the particles and thus on the final identification of the type of reaction. They also yield the energy of the incident neutron.

For a p-type event these equations become

$$T_n = T_n \left(\sum_j p_{xj} + p_{n'x}\right) = \sum_j T_j + Q + T_n' ,$$

$$p_{n'y} = - \sum_j p_{yj} ,$$

$$p_{n'z} = + \sum_j p_{zj} .$$

Combining these with the kinematical relation between the energy and momentum of a neutron, one arrives at the energy of the incident neutron as well as the energy and direction of the outgoing neutron.

Unfortunately the inaccuracies of measurement make the identification of the particles uncertain in many cases. Indentification by momentum–energy balance and identification by relative ionization both depend upon good measurements of ρ, the radius of curvature of the track. Two factors influence the accuracy of a ρ measurement. They are turbulence in the cloud chamber, and the length of the track. Multiple measurements have led to the criterion that the sagitta of a uniform track can be read to 0.1 mm. Poor tracks, such as those that are tapered by virtue of leaving the illuminated region, cannot be measured this accurately. Final identification of each particle--and therefore of the type event--is made with these errors taken into account. If the errors are such as to make a positive identification impossible the event is listed as a questionable one of the most probable type. This breakdown is discussed further in a section on questionable-type events.

Dip Angle Limiations

Because of measuring difficulaties, meson events in which the pion had a dip angle greater than $\alpha_o = 50^o$ were excluded from the data. For this reason a geometric correction factor $f(\theta, \alpha_o)$, as given in Table III, had to be applied to each event. Two assumptions were made in its derivation and use. The first is that pion production is azimuthally symmetric about the beam direction, and the second is that for each event in which the pion has an angle θ, there are $\left[1-f(\theta, \alpha_o)\right]$ identical events in which the pion is in the excluded region. The former assump-

tion means that $f(\theta, \alpha_o)$ is simply the ratio of the total solid angle to the available, or unexcluded, solid angle for a given θ and α_o. The latter means that this factor is applied to all properties of the event as a whole, i.e. $f(\theta, \alpha_o)$ is applied not only to the pion angular distribution but also to its energy spectrum as well as the proton angle and energy distributions.

No other correction factor was needed, as it was not necessary to exclude events whose positive particles had steep dip angles. This follows because the deuterons and He^3's could not have steep dip angles, and those protons having steep dip angles had low energies, making accurate measurements on them unnecessary.

EXPERIMENTAL CHECKS AND DISCUSSION OR ERRORS

As mentioned in the introduction, several symmetry checks were made to ascertain whether events having particular characteristics might be missed. This chapter is devoted to these checks, the checks on the assumption of azimuthal symmetry, and a discussion of systematic errors.

Azimuthal Symmetry Check

As a test of azimuthal symmetry, the pions were grouped in eight angular groups or octants of ϕ as defined in Fig. 7A. Table V lists the number of events falling into each group by run number, the total number in each octant, and the number that fell in the excluded region for all runs.

Subtracting the total number of events from the corrected number, we get the number that should have fallen into the excluded regions. This number (63.3) is to be compared with the actual number (53) found in the excluded region, and they seem to be in fair statistical agreement. Dividing the 63.3 equally among the four octants containing the excluded region, and adding this to the total number in each octant,* we get the graph of Fig. 7B, where in the errors shown are the statistical standard deviations. If the total corrected number of events were divided equally among the eight octants, the horizontal line in Fig. 7B would be obtained. This figure indicates an asymmetry between pions going up and those going down, but good agreement between those going up and those going down, each considered alone.

Table V also makes two other comparisons using the azimuthal angles. In the first, pions going to the right (Octants 3, 4, 5, and 6) are compared with those going to the left (Octants 1, 2, 7, and 8), and in the second, pions going up (Octants 5, 6, 7, and 8) are compared with those going down (Octants 1, 2, 3, and 4). The actual number of events is recorded rather than the corrected number, since the excluded regions are symmetric in both cases. It is seen that the right-left symmetry is excellent, and that the only possible asymmetry is up and down (as also indi-

* 16 was used although 63.3/4 = 15.8

Table V

Azimuthal Distributions

φ Octant	φ Interval	Total Number of Pions in φ Octants; $\alpha \geq 50^\circ$ Excluded: Run Numbers 0	1	2	5	6	Total All Runs	Total Number Found With $\alpha \geq 50^\circ$ In All Runs	Corrected Number With $\alpha \geq 50^\circ$ from $1-f(\theta,\alpha_0)$	Total Corrected Number In Each Octant
1	0° 45°	2	15	10	11	14	52	--	--	52 ± 7.2
2	45° -90°	0	7	9	5	17	38	15	16	54 ± 8.8
3	90°-135°	0	7	10	8	12	37	17	16	53 ± 8.7
4	135°-180°	1	15	10	14	17	57	--	--	57 ± 7.6
5	180°-225°	1	14	11	4	10	40	--	--	40 ± 6.3
6	225°-270°	1	6	2	7	4	20	7	16	36 ± 8.1
7	270° -315°	3	8	4	2	5	22	14	16	38 ± 8.1
8	315°-360°	0	11	10	9	14	44	--	--	44 ± 6.6
Right	90°-270°	3	42	33	33	43	154			
Left	0°-90° and 270°-360°	5	41	33	27	50	156			
Up	180°-360°	5	39	27	22	33	126			
Down	0°-180°	3	44	39	38	60	184			

cated above). The up-down asymmetry is possibly not statistical, and as a check to be sure that particular types of events are not being missed, θ distributions for pions going up are compared with those for pions going down in a later section of this chapter. Similar distributions are also made there for the energy spectra.

It may also be noted that the ϕ distribution for each run has the same general appearance within statistics, so that no ϕ asymmetry is apparent for any individual run.

Those events listed in Table V which have $\alpha \geq 50^{\circ}$ are discussed in this section only. In all other sections the corrected numbers from $f(\theta, \alpha_o)$ are used.

Distribution of Origins

In order to establish whether events produced in one region of the cloud chamber were more likely to be missed than those in another, the collimated region of the cloud chamber was divided into twelve boxes along the beam direction. These boxes, or regions, are illustriated in Fig. 8A as they would appear to someone looking down upon the cloud chamber Regions B, C, F, and G are all the same size as one another but twice as large as the other regions. In order that the various regions may be directly compared, the normalized column of Table VI lists the actual* number of events occuring in regions B, C, F, and G and twice the actual number in the other regions. The errors shown are the statistical standard deviations.

The X regions (A_x, D_x, E_x, and H_x) are separated from the others in Table VI because they are considered in this section alone. One of the purposes of this section is to show that events in the X regions are unreliable. This is not unexpected, because in D_x and H_x the tracks were short and pions in the forward direction might very easily have been missed. In regions A_x and E_x the backwards ones are the most earily missed. Therefore pions in the vicinity of 90° may possibly be favored over those going forward and backward if the X sections

---

* Since exclusion of dip angles greater than or equal to 50° affects all regions symmetrically, the actual number of events rather than the corrected number is used.

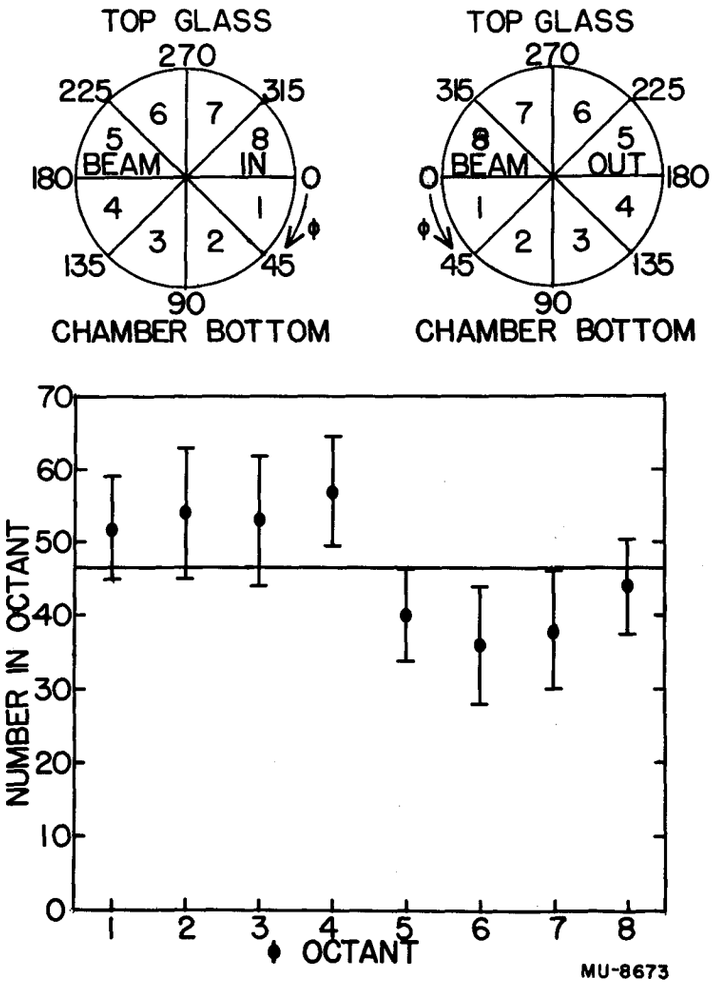

Figs. 7(A) and 7(B) Definitions of the ϕ octants; 7(C) azimuthal distribution plot.

are included. Another reason for excluding regions D_x and H_x is that the positive tracks are so short that it is impossible to identify events either by momentum balance or ionization, and they would all have to be lumped into the questionable category, discussed in a later section of this chapter.

Table VI

Left Half of Chamber			Right Half of Chamber		
Region	Actual Number	Normalized Number	Region	Actual Number	Normalized Number
A	17	34 ± 8.2	E	16	32 ± 8.0
B	49	49 ± 7.0	F	52	52 ± 7.2
C	58	58 ± 7.6	G	69	69 ± 8.3
D	27	54 ±10.4	H	22	44 ± 9.4
Sum	151	195 ±15.9	Sum	159	197 ±15.6
A_x	16	32 ± 8.0	E_x	5	10 ± 4.5
D_x	19	38 ± 8.7	H_x	9	18 ± 6.0
X Sum	35	70 ±11.8	X Sum	14	28 ± 7.5

Fig. 8B is a plot of the data given in Table VI. The upper horizontal line in the figure corresponds to dividing the 310 events of Regions A to H uniformly among these regions with proper normalization, and the lower line corresponds to dividing the 359 events of all regions uniformly throughout and normalizing. It is seen that if Regions X are excluded the average lies within 5 of the 8 standard deviations, whereas a similar analysis of all regions yields 5 out of the 12 within the standard deviations. This analysis shows therefore that the x regions are unreliable.

Returning to Table VI, one may notice that the right-left symmetry is excellent except in the X regions. Therefore the right and left

data are added and the regions are renumbered as shown in Fig. 9A. The results of this step are shown in Table VII and Fig. 9B. Again the upper horizontal line of Fig. 9B corresponds to the average number of events in each region if the X regions are excluded and the lower line to the average if all regions are included. The fact that the average falls

Table VII

Region	2 A + E	3 B + F	4 C + G	5 D + H	1 $A_x + E_x$	6 $D_x + H_x$
Actual No. in Region	33	101	127	79	21	28
Normalized No. in Region	66 ±11.5	101 ±10.0	127 ±11.3	98 ±14.0	42 ±9.2	56 ±10.6

within only 1 out of 6 of the standard deviations if all the data are included, and within 2 out of 4 if Regions X are excluded, adds greatly to the above arguments for excluding the X regions, and this has been done throughout the remainder of the paper.

As one further check, Table VIII compares the total number in the forward half of the chamber (the beam-exit half) with the total number in the backward half. These are the actual numbers, since the regions are the same size. The indication from Table VIII is that events may have been missed in the backward regions, but this could have been a statistical fluctuation. Since the forward half of the chamber does have less background and is easier to scan, a later section of this chapter compares the pion angle and energy distributions in the two halves to ascertain whether or not any difference is apparent.

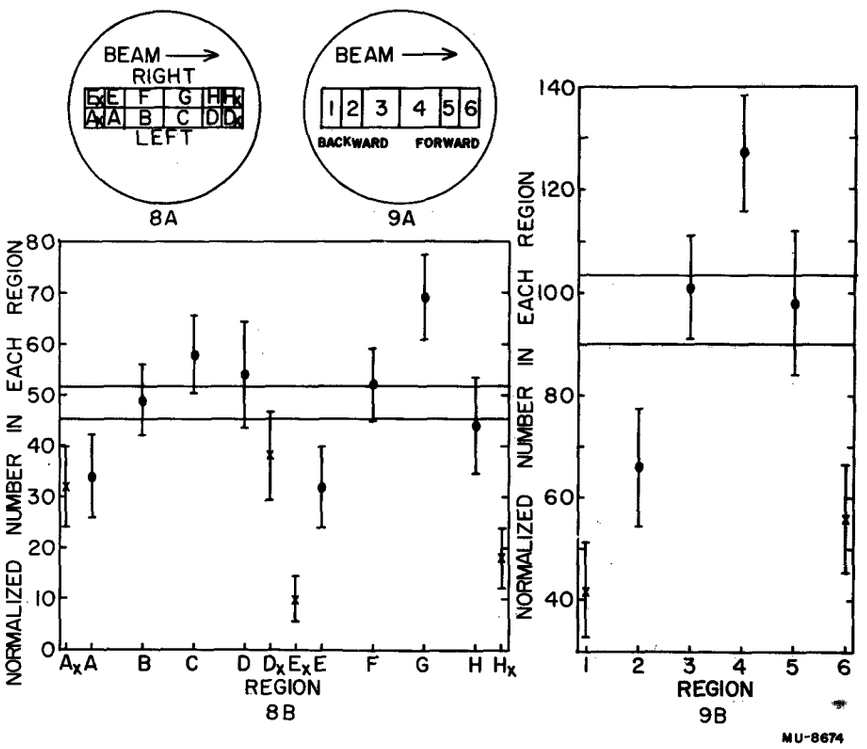

Figs. 8(B) and 9(B) Definitions of regions as seen by looking down on the cloud chamber; Figs. 8b and 9b, regional distribution plots.

Table VIII

Actual Number of Events in Forward and Backward Halves of Chamber (Regions X Excluded)

Forward	176 ± 13
Backward	134 ± 12

As a final check, Table IX breaks the regional distribution down by runs, listing the actual number of events in each region. No thorough analysis was made of each run because of the small numbers involved, but the trends on a run-to-run basis seem to be the same as those of the totals.

Table IX

	Region							
Run No.	A	B	C	D	E	F	G	H
0	1	1	0	1	0	1	2	2
1	4	15	17	11	4	3	23	6
2	3	8	16	3	0	14	17	5
5	5	8	5	4	9	19	6	4
6	4	17	20	8	3	15	21	5
Totals	17	49	58	27	16	52	69	22

Checks on Angular and Energy Distributions

Since the last two sections have indicated possible asymmetries between events found in the forward and backward halves of the cloud chamber, and between events for which the pion goes up or down, this section compares pion energy and angular distributions within these breakdowns.

Pion Up vs. Pion Down Distributions

Table X compares the number of pions going up with those going down by angular intervals. Both the actual and corrected number (N and N_c) of pions in each interval are listed, as are the statistical standard deviations on the corrected number. The data are plotted in Fig. 10 where, in order to distringuish the two sets of data, those points corresponding to mesons going down are plotted one division to the left of center and those corresponding to mesons going up are plotted one division to the right. Since the purpose is only to compare the two sets of data, solid-angle corrections are not included in this graph.

Breaking the pion energy distributions down in an exactly similar manner, we get Table XI and Fig. 11.

Since the two energy spectra are very similar and both angular distributions have the same general shape, no up-down asymmetry is apparent.

Distribution For Forward vs. Backward Chamber Halves

If we follow the above procedure but make the breakdown according to whether the origins lie in the forward or backward halves of the chamber, we get the results of Table XII and Fig. 12 for the pion angular distributions and those of Table XIII and Fig. 13 for the energy spectra. Again we see no essential differences and assume there are no important forward-backward asymmetries.

The Questionable Events

Two distinctly different categories of questionable events are discussed in this section. Considered first are those events in which, although a pion definitely has been produced, the type of event is in ques-

Table X

θ	Number of Pions Going			
	Down		Up	
	N	N_c	N	N_c
0 - 9.4	11	11.0±3.3	1	1.0± 1.0
9.5 - 19.4	25	25.0±5.0	14	14.0± 3.7
19.5 - 29.4	33	33.0±5.7	22	22.0± 4.7
29.5 - 39.4	25	25.0±5.0	13	13.0± 3.6
39.5 - 49.4	19	19.0±4.4	18	18.0± 4.2
49.5 - 59.4	12	15.5±4.5	11	14.1± 4.2
59.5 - 69.4	11	17.2±5.2	8	12.3± 4.3
69.5 - 79.4	10	16.9±5.4	5	8.6± 3.9
79.5 - 89.4	7	12.4±4.7	10	17.8± 5.6
89.5 - 99.4	7	12.5±4.7	6	10.7± 4.4
99.5 - 109.4	4	6.9±3.5	5	8.7± 3.9
109.5 - 119.4	2	3.2±2.2	2	3.0± 2.2
119.5 - 129.4	7	8.9±3.4	5	6.7± 3.0
129.5 - 139.4	4	4.0±2.0	3	3.0± 1.7
139.5 - 149.4	5	5.0±2.2	2	2.0± 1.4
149.5 - 159.4	0	0	1	1.0± 1.0
159.5 - 169.4	1	1.0±1.0	0	0
169.5 - 180	1	1.0±1.0	0	0

Table XI

T_π (Mev)	Number of Pions Going Down		Number of Pions Going Up	
	N	N_c	N	N_c
0 - 9.4	21	27.0 ± 5.9	21	30.9 ± 6.7
9.5 - 19.4	35	46.0 ± 7.8	18	24.7 ± 5.8
19.5 - 29.4	26	31.8 ± 6.2	20	24.6 ± 5.5
29.5 - 39.4	26	31.4 ± 6.2	18	23.0 ± 5.4
39.5 - 49.4	12	13.0 ± 3.8	16	19.1 ± 4.8
49.5 - 59.4	22	25.6 ± 5.5	10	10.3 ± 3.3
59.5 - 69.4	16	16.5 ± 4.1	12	12.0 ± 3.5
69.5 - 79.4	7	7.0 ± 2.6	6	6.2 ± 2.5
79.5 - 89.4	6	6.0 ± 2.4	3	3.0 ± 1.7
89.5 - 99.4	7	7.0 ± 2.6	0	0
99.5 - 109.4	3	3.0 ± 1.7	1	1.0 ± 1.0
109.5 - 119.4	2	2.0 ± 1.4	1	1.0 ± 1.0
119.5 - 129.4	1	1.3 ± 1.3	0	0

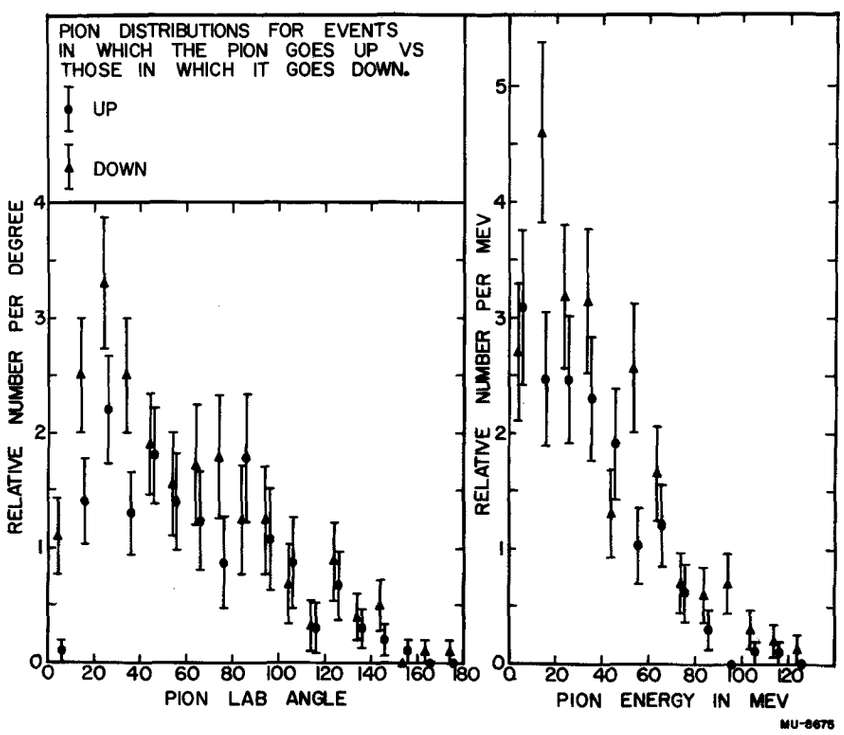

Figs. 10 and 11 Angular and energy distributions comparion pions going up (towards the top glass) with those going down. So that they don't overlap, the points corresponding to pions going up are plotted one division to the right of center and those going down one division to the left of center.

Table XII

θ	Number of Pions Whose Origins Lie in the Forward or Backward Halves of the Cloud Chamber			
	Forward		Backward	
	N	N_c	N	N_c
0 - 9.4	3	3.0 ± 1.7	9	9.0 ± 3.0
9.5 - 19.4	20	20.0 ± 4.5	19	19.0 ± 4.4
19.5 - 29.4	26	26.0 ± 5.1	29	29.0 ± 5.4
29.5 - 39.4	14	14.0 ± 3.7	24	24.0 ± 4.9
39.5 - 49.4	14	14.0 ± 3.7	23	23.0 ± 4.8
49.5 - 59.4	11	13.6 ± 4.1	12	16.0 ± 4,6
59.5 - 69.4	10	15.4 ± 4.9	9	14.1 ± 4.7
69.5 - 79.4	4	6.8 ± 3.4	11	18.8 ± 5.7
79.5 - 89.4	9	16.0 ± 5.3	8	14.2 ± 5.0
89.5 - 99.4	6	10.7 ± 4.4	7	12.5 ± 4.7
99.5 - 109.4	4	6.9 ± 3.5	5	8.7 ± 3.9
109.5 - 119.4	3	4.7 ± 2.7	1	1.5 ± 1.5
119.5 - 129.4	4	5.1 ± 2.5	8	10.5 ± 3.7
129.5 - 139.4	2	2.0 ± 1.4	5	5.0 ± 2.2
139.5 149.4	4	4.0 ± 2.0	3	3.0 ± 1.7
149.5 159.4	0	0	1	1.0 ± 1.0
159.5 - 169.4	0	0	1	1.0 ± 1.0
169.5 - 180	0	0	1	1.0 ± 1.0

Table XIII

T_π (Mev)	Number of Pions Whose Origins Lie in the Forward or Backward Halves of the Cloud Chamber			
	Forward		Backward	
	N	N_c	N	N_c
0 - 9.4	17	21.8 ± 5.3	25	36.1 ± 7.2
9.5 - 19.4	34	46.2 ± 7.9	19	24.5 ± 5.6
19.5 - 29.4	28	35.0 ± 6.6	18	21.4 ± 5.0
29.5 - 39.4	28	33.5 ± 6.3	16	21.0 ± 5.3
39.5 - 49.4	16	17.8 ± 4.5	12	14.3 ± 4.1
49.5 - 59.4	20	23.0 ± 5.1	12	12.8 ± 3.7
59.5 - 69.4	15	15.5 ± 4.0	13	13.0 ± 3.6
69.5 - 79.4	5	5.2 ± 2.3	8	8.0 ± 2.8
79.5 - 89.4	5	5.0 ± 2.2	4	4.0 ± 2.0
89.5 - 99.4	4	4.0 ± 2.0	3	3.0 ± 1.7
99.5 - 109.4	2	2.0 ± 1.4	2	2.1 ± 1.4
109.5 - 119.4	1	1.0 ± 1.0	2	2.0 ± 1.4
119.5 - 129.4	1	1.3 ± 1.1	0	0

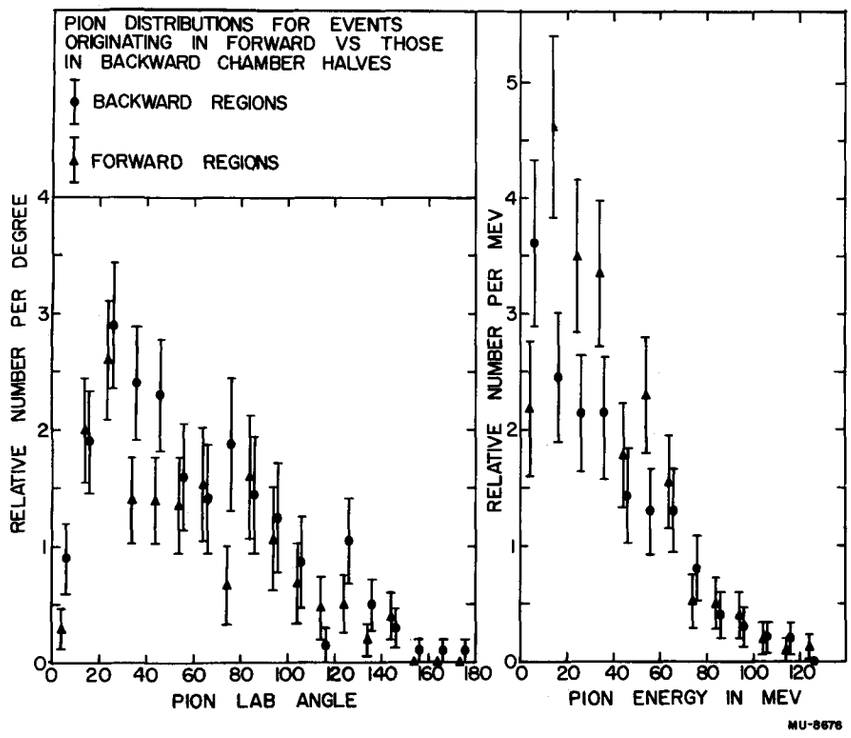

Figs. 12 and 13 Pion angular and energy distributions comparing events whose origins lie in the forward half (or beam exit half) of the cloud chamber with those whose origins lie in the backward half. Here the points corresponding to the forward regions are plotted one division to the left of center whereas the backward region points are plotted one division to the right of center

tion. The second category consists of the two-prong stars, i.e., stars that appear as if they should have a meson associated but do not.

The Questionable-Type Event

An event might be labeled a questionable type for any of several reasons. The predominant reason was that one or more of the tracks was too short to measure curvature accurately. Short tracks were caused by various things. One was lack of water vapor near the top glass, a difficulty that arose in a few pictures where the cycle time was too short. Scattering also effectively shortened the region over which the curvature of a track could be measured. Tracks starting near the beam-exit section of the chamber can be seen for only a short distance. Turbulence also made the "questionable" label necessary in a few events, as did a dot in coincidence with the origin. The dot raised the question of whether the star was really a meson produced in deuterium or in oxygen with the dot being the recoiling oxygen nucleus. Two events having dots at the origins were included in the final data. One of these, since momentum-energy balance and ionization were in good agreement, was labeled as a d-type event. The other was labeled a questionable p-type, since it could be balanced as a p-type, but remained questionable because balance does not exclude the residual oxygen nucleus from carrying off momentum in this case as it does in the d event above. Also it is not unreasonable to assume that these dots might have been coincidences, as there are many dots of the same general size throughout the pictures.

These questions may arise from either of these indications: lack of momentum-energy balance, or balance with an energy for the incident neutron above the maximum beam energy (340 Mev). By "balance" (in the above and following statements) is meant transverse momentum balance as well as forward momentum-energy balance for the d and He^3 type events, and the same balance within the neutron-energy limits set by threshold and maximum beam energy for a p-type event. Balance therefore is not as restrictive in a p- as in a d- or He^3-type event. If balance was not achieved in the original measurements* an attempt was made to

* All events were measured twice, and those having important disagreements between the measured values were measured a third time before the calculations were performed. Weighted averages of these measurements were used in the calculations and are referred to as the original measurements.

bring about a balance within the limits of measurement errors. When this was possible the event was placed in the completed stack as the type event it balanced out to be, or--if it could be balanced as more than one type within the measured errors and more precise measurements could not be hoped for--it was labeled a questionable event of the type to which it most probably belonged.

In case balance could not be achieved within the measured values, or if balance indicated that the type was different from that obtained by ionization, an independent remeasurement was made on the event. After this remeasurement the calculations were compared directly with the tracks to determine if possibly a small-angle scatter made the track appear more or less curved than it actually was. Also noted at this time was any possible turbulence. If agreement could then be obtained between ionization and balance, or if the assumption of about 20-meter turbulence* would make the event qualify as one type but not as another, the classification was considered completed.

Those events still remaining were listed as questionable ones of the most probable type, and the chief purpose of this section is to justify lumping these events with the unquestionable ones. Before leaving the discussion of how the events were classified, however, it should be remarked that no sharp boundary existed between questionable and unquestionable, and possibly a few of each could actually be interchanged.

In Table XIV the 310 events used in the final results of this paper are broken down as to type of event, and as to whether they were questionable or not. It is seen that one out of ten events of each type was questionable. As He^3's cannot be confused with the other types of event, they are labeled questionable only because their balance was not as good as might be expected. This follows since a He^3 event consists of one very black, straight positive track and one light negative track--a distinctively different appearance from the other types of event.

---

* By 20 meter turbulence one means that a track would have an average radius of curvature of 20 meters if there were no magnetic field.

Table XIV

Type Event	Unquestionable	Questionable	Ratio: Questionable to Unquestionable	Total Questionable and Unquestionable
d	185	23	0.12	208
p	74	6	0.08	80
He^3	19	3	0.16	22
Totals	278	32	0.12	310

One might conclude therefore, on the basis that the ratios of questionables to unquestionables for the three types of event are the same, that the events are grouped approximately correctly.

In order to determine if any systematic errors would be introduced by adding the questionables to the unquestionables, Table XV compares the energy and angular distributions of the d type with the questionable d type. As used previously, N is the actual number in the interval, and N_c the corrected number. For comparison purposes the corrected number in the questionable column is normalized by the ratio of the total number of unquestionables to questionables of the d type. It is seen that only 2 out of 18 points in the angular distribution of Table XV do not overlap, whereas 7 out of 12 do not overlap in the energy spectra. This seems probably as good an agreement as can be expected from the small numbers involved. The questionable numbers are so small in the other two cases that tables similar to Table XV would be meaningless for them. The only conclusion we can draw from the meager statistics is that adding the questionables to the unquestionables does not introduce any apparent systematic error. It might also be noted that it seemed more reasonable to add in the questionables than to discard them for the following two reasons : (a) it is highly probable that most of the question-

Table XV

Comparison of Distributions for Questionable and Unquestionable Events in the Reaction, $n + d \rightarrow \pi^- p + d$

	Unquestionables		Questionable	
θ	N	N_c	N	8.0 N_c
0 - 9.4	9	9.0 ± 3.0	2	16 ± 11
9.5 - 19.4	24	24.0 ± 4.9	2	16 ± 11
19.5 - 29.4	34	34.0 ± 5.8	2	16 ± 11
29.5 - 39.4	27	22.0 ± 4.7	2	16 ± 11
39.5 - 49.4	23	23.0 ± 4.8	2	16 ± 11
49.5 - 59.4	10	13.2 ± 4.2	1	9 ± 9
59.5 - 69.4	8	12.5 ± 4.3	3	37 ± 21
69.5 - 79.4	9	15.3 ± 5.1	1	14 ± 14
79.5 - 89.4	11	19.6 ± 5.9	3	43 ± 25
89.5 - 99.4	9	16.0 ± 5.3	1	14 ± 14
99.5 -109.4	6	10.4 ± 4.2	2	28 ± 20
109.5 -119.4	1	1.6 ± 1.6	1	12 ± 12
119.5 -129.4	8	10.5 ± 3.9	1	11 ± 11
129.5 -139.4	4	4.0 ± 2.0	-	-
139.5 -149.4	5	5.0 ± 2.2	-	-
149.5 -159.4	1	1.0 ± 1.0	-	-
159.5 -169.4	1	1.0 ± 1.0	-	-
169.5 -180	-	-	-	-

	Unquestionables		Questionable	
T_π(Mev)	N	N_c	N	8.0 N_c
0 - 9.4	24	34.0 ± 6.9	3	37 ± 21
9.5 - 19.4	30	38.9 ± 7.1	7	87 ± 33
19.5 - 29.4	30	37.4 ± 6.8	2	20 ± 14
29.5 - 39.4	22	28.4 ± 6.1	4	35 ± 18
39.5 - 49.4	16	18.9 ± 4.7	4	33 ± 16
49.5 59.4	23	24.6 ± 5.1	3	35 ± 20
59.5 - 69.4	16	16.0 ± 4.0	-	-
69.5 - 79.4	8	8.0 ± 2.8	-	-
79.5 - 89.4	6	6.0 ± 2.4	-	-
89.5 - 99.4	6	6.0 ± 2.4	-	-
99.5 -109.4	2	2.0 ± 1.4	-	-
109.5 -119.4	2	2.0 ± 1.4	-	-

ables were correctly classified as to type, (b) throwing out questionables would have made the boundary between questionable and unquestionable events very important, and one would have to be extremely careful to not introduce systematic errors by excluding events of all the same type.

The Questionable Two-Prong Stars

As mentioned in a previous discussion on scanning, there are several possible explanations of two-prong stars. All those which probably could not have been meson stars (for any one of various reasons) have been eliminated from this discussion. Also eliminated are those stars with origins in the X regions and those for which the pion, if it existed, would have to have a dip angle $\geq 50^{\circ}$ in order to balance momentum. After a thorough analysis, only 11 stars could not be positively eliminated as possible meson events. Some of these are almost certainly events where the pion is unseen for one reason or another, and still others probably could not be events. Fortunately, however, these 11 stars amount to only 3.8% of the total number of p- and d-type events found, and therefore introduce a negligible error.

Scanning Errors

The film scanning was accomplished by two observers one of whom (referred to as No. 2) scanned only part of the film, whereas the other (No. 1) scanned all the film and rescanned that part not scanned by No. 2. The scanning by No. 2 and the rescanning by No. 1 is all referred to as rescanning even though in many instances No. 2's observations preceded No. 1's in time. Table XVI lists by run Nos. the known number of events in the section on film scanned by each observer, the number of these events which that observer missed, and the scanning efficiency calculated thereby. It also illustrates the totals of each of these quantities for all runs.

Table XVI

Scanning Efficiencies

Observer Number	Run No.	0	1	2	5	6	Total
1	Number Scanned	8	83	66	60	93	316
	Number Missed	0	5	8	4	11	28
	Efficiency %	100	94	88	93	88	91
2 *	Number Scanned	8	83	47	2	72	212
	Number Missed	3	14	6	0	10	33
	Efficiency %	62	83	87	100	86	84
1 *	Number Scanned	0	0	19	58	19	96
	Number Missed	0	0	1	3	4	8
	Efficiency %	-	-	95	95	79	92

* Rescanning

As the run-by-run efficiency of each observer does not differ appreciably from their total efficiency, and as the efficiencies of both observers are approximately equivalent, these results have been combined to yield Table XVII. If the probability of missing an event is scanning is purely statistical, the probability that it will be missed in two independent scannings is the product of the two individual probabilities. Therefore the scanning and rescanning inefficiencies are also listed in Table XVII, as are the total inefficiency.

Table XVII

Combined Scanning and Rescanning Efficiencies

	Efficiency	Inefficiency
Scanning	91%	9%
Rescanning	87%	13%
Combined Results	98.8%	1.2%

This result indicates that probably only one meson in a hundred was missed. This is of course a negligible number, but it is still necessary to ascertain whether the events missed were missed for statistical reasons(as was assumed for the above calculation) or whether the harder ones to find were missed most frequently. As a check on this the angular and energy distributions of those pions missed (N_m) by one of the observers are compared with those not missed ($N - N_m$) at all in Table XVIII, where, for comparison, the total number missed is normalized to the total number not missed. Since the standard deviations for all but 4 of the 13 evergy distribution points and 1 out of 18 angular distribution points overlap, it is concluded that mesons of particular angles or energies were not missed.

The only other possibility to be considered is whether events of a particular type were missed more frequently than another type. As a test of this the upper half of Table XIX lists the total number (N) of events of each type found, with questionables and unquestionables separated; the total number (N_m) of each type missed by one observer or other; and their difference, the number not missed at all. The ratio of the total number of questionables to unquestionables is essentially the same in both cases (14% for those missed and 11% for those not missed); and they have therefore been combined in the bottom half of that table. Also, for comparison purposes, a column has been added that normalizes the total number missed to the total number not missed, and the statistical probable errors are given on both of these.

Table XVIII

Comparison of Pion Distributions for Missed vs. Unmissed Events

Angular Distribution					
θ		N	N_m	$N-N_m$	$3.63\ N_m$
0 -	9.4	12	4	8 ± 2.8	14.5 ± 7.2
9.5 -	19.4	39	9	30 ± 5.5	32.7 ± 10.9
19.5 -	29.4	55	14	41 ± 6.4	50.8 ± 13.6
29.5 -	39.4	38	9	29 ± 5.4	32.7 ± 10.9
39.5 -	49.4	37	10	27 ± 5.2	36.3 ± 11.5
49.5 -	59.4	23	5	18 ± 4.2	18.2 ± 8.1
59.5 -	69.4	19	4	15 ± 3.9	14.5 ± 7.2
69.5 -	79.4	15	1	14 ± 3.7	3.6 ± 3.6
79.5 -	89.4	17	2	15 ± 3.9	7.3 ± 5.2
89.5 -	99.4	13	2	11 ± 3.3	7.3 ± 5.2
99.5 -	109.4	9	1	8 ± 2.8	3.6 ± 3.6
109.5 -	119.4	4	1	3 ± 1.7	3.6 ± 3.6
119.5 -	129.4	12	2	10 ± 3.2	7:3 ± 5:2
129.5 -	139.4	7	2	5 ± 2.2	7.3 ± 5.2
139.5 -	149.4	7	1	6 ± 2.5	3.6 ± 3.6
149.5 -	159.4	1	0	1 ± 1	0
159.5 -	169.4	1	0	1 ± 1	0
169.5 -	180	1	0	1 ± 1	0

Energy Spectrum					
T_π(Mev)		N	N_m	$N-N_m$	$3.63\ N_m$
0 -	9.4	42	2	40 ± 6.3	7.3 ± 5.2
9.5 -	19.4	53	9	44 ± 6.7	32.7 ± 10.9
19.5 -	29.4	46	4	42 ± 6.5	14.5 ± 7.2
29.5 -	39.4	44	10	34 ± 5.8	36.3 ± 11.5
39.5 -	49.4	28	5	23 ± 4.8	18.2 ± 8.1
49.5 -	59.4	32	11	21 ± 4.6	40.0 ± 12.1
59.5 -	69.4	28	11	17 ± 4.1	40.0 ± 12.1
69.5 -	79.4	13	4	9 ± 3.0	14.5 ± 7.2
79.5 -	89.4	9	4	5 ± 2.2	14.5 ± 7.2
89.5 -	99.4	7	3	4 ± 2.0	10.9 ± 6.3
99.5 -	109.4	4	2	2 ± 1.4	7.3 ± 5.2
109.5 -	119.4	3	1	2 ± 1.4	3.6 ± 3.6
119.5 -	129.4	1	1	0	3.6 ± 3.6

Table XIX

Comparison of Event Types for
Those Missed and Those Not Missed

	Type Event	N	N_m*	N - N_m	3.63 N_m
Unquestionables	d	185	37	148	
	p	74	11	63	
	He^3	19	11	8	
	Total	278	59	219	
Questionables	d	23	3	20	
	p	6	2	4	
	He^3	3	3	0	
	Total	32	8	24	
Questionables & Unquestionables Combined	d	208	40	168 ± 13	145 ± 23
	p	80	13	67 ± 8	47 ± 13
	He^3	22	14	8 ± 3	51 ± 14

* The total numbers missed in this table do not equal the total numbers missed in Tables XVI and XX, because two events (one of these a He^3) were missed in both scanning and rescanning, and were found in independent checks that were not systematic and cound not be given efficiencies. The 2 missed out of 310 is not in disagreement with the 1% calculated above, however.

From Table XIX it is apparent that the He^3 events are more likely to be missed in scanning, than the others, and that the 1 in 100 missed as calculated above can only be applied to the deuteron- and proton-type events.

In order to obtain a total scanning efficiency for the He^3's, Table XX combines the pertinent information of Tables XVI and XVII for the He^3 events alone. The results indicate that approximately 11% of the He^3-type events could have been missed, implying that the ratio of He^3's to the total number as given in the results could have a systematic error of 11%, but this error is completely dwarfed by the statistical error on the 22 events and is therefore of no great importance.

Table XX

Combined Scanning and Rescanning
Efficiencies for He^3 Events

	N	N_m	Efficiency	Inefficiency
Scanning	22	8	64%	36%
Rescanning	22	7	68	32%
Combined Results			89%	11%*

* The one event missed in common, see foot-note to Table XIX, out of 22 possible is not in disagreement with this, but it was found in a non-systematic check and cannot be given an efficiency.

Errors in Measurement of Pion Energy

The sources of error in pion-energy measurements are the same as those leading to lack of momentum balance in the section entitled The Questionable-Type Event. They are short tracks and turbulence. The lengths of the pion tracks were such, on the average, as to give an uncertainty in the pion momentum of about ±5%. The assumption of 1 meter turbulence, which was the worst value in this cloud as determined by De Pangher[10] for steep tracks, would yield only a ±2% error in the momentum of a pion of mean energy. The momentum-balance results of this experiment indicate that tracks near the horizontal in general are not subject to more than 20 meters turbulence; therefore momentum errors greater than ±2% due to turbulence are exceptions and total pion momentum errors are of the order of ±5%. This means that the pion-energy errors are only of the order of 10% on the average.

Errors in Measurement of Neutron Energy

In order to estimate the errors involved in neutron-energy measurements, Table XXI lists the number of d and He^3 events in each energy interval that have estimated errors of ±3%, ±6%, and ±10%. Because these were obtained from the degree of balance or unbalance, similar estimates could not be made on the p events. The errors in the neutron

energies for the p-type events are certainly of the same order as for the d events, however. The total numbers with ±3%, ±6% and ±10% in the d-type event can be fitted to a gaussian of 8.3% standard deviation.

Total Cross Section

As a final check to ascertain if the number of events found was consistent with the number of neutrons going through the chamber and the total cross section for pion production, this cross section was calculated for the data of Run 2 by the two methods given by Ford.[12] The first of these methods used an ionization chamber, which was calibrated by comparison with the neutron-proton scattering results of DePangher.[10] The second method involved counting the total number of oxygen stars and deriving the cross section from the inelastic cross section for neutrons on oxygen and the relative numbers of oxygen and deuterium nuclei in the cloud chamber. The first method led to a cross section of about 0.3 millibarn, and the second to 0.1 millibarn. It should be noted that these numbers are subject to large systematic errors and are included only to show that they are of the right order of magnitude as predicted by charge independence.

Table XXI

Neutron-Energy Errors

	$n + d \rightarrow \pi^- + p + d$			$n + d \rightarrow \pi^- + He^3$		
	Number With Energy Error Approx. Equal To			Number With Energy Error Approx. Equal To		
T_n (Mev)	±3%	±6%	±10%	±3%	±6%	±10%
220	-	-	-	1	-	-
230	-	-	-	-	-	-
240	-	-	-	1	-	-
250	1	-	-	1	-	-
260	-	-	2	2	-	-
270	4	6	2	1	2	-
280	9	6	-	1	1	-
290	8	10	2	2	-	2
300	25	13	7	3	1	-
310	24	13	-	-	-	-
320	22	13	5	-	1	-
330	9	7	2	1	1	-
340	4	5	9	-	1	-
Totals	106	73	29	13	7	2

RESULTS AND CONCLUSIONS

Ideally the results of this experiment should be presented in the form of pion angular and energy distributions in the center-of-mass system for the two colliding neutrons.* Because this center-of-mass system is not known it was deemed best to present the laboratory-system distributions as derived from known deuteron wave functions and various assumed center-of-mass-system distributions. At the present time a calculation of this type is being carried out under the impulse approximation, using the following assumptions:[15]

(a) Only the neutron-neutron interaction gives the pion and the deuteron, i.e. the final deuteron is formed from the initial colliding neutrons.

(b) The excitation function given by Schultz[16] for proton-proton π^+ production is valid for neutron-neutron π^- production.

(c) The only function of the initial proton is to provide a momentum distribution for the neutron in the deuteron.

(d) The deuteron momentum wave function is gaussian.

(e) The neutron spectrum is that given by DePangher[10].

(f) The center-of-mass-system angular distribution either is symmetric of equals $\left[1/3 + \cos^2\theta.\right]$. Both cases are being carried out for comparison purposes.

One fault with this theory is immediately obvious. This concerns the protons in the deuteron-type reactions. They should be directed

---

* At 400 Mev the reaction $p + p \rightarrow \pi^+ + d$ is favored over the reaction $n + p \rightarrow \pi^- + 2p$ by a factor of 7.6.[14] Therefore the proton in the d could produce only about 10% of the events and this would not be detectable within the statistics of this experiment.

essentially forward* with energies corresponding to the momenta they would have in the deuteron, and it is noted that their angular distribution does agree substantially with this, but the high-energy protons cannot be accounted for by the model given. Because these proton distributions do provide a test for any theory on the deuteron-type reaction, they have been included in the results, Table XXIV.

The pion laboratory-system differential cross sections for the three reactions are presented in Table XXII and plotted in Figs. 14, 15, and 16. Similarly Table XXIII and Figs. 17, 18, and 19 give the pion laboratory-system energy spectra. The distributions for the protons in deuteron-type events are tabulated in Table XXIV. The relative frequencies of the three types of events are represented in Table XXV. In all cases N equals the actual number of events observed and N_c the corrected number of $\alpha \geq 50^\circ$ being discarded. The scales are all arbitrary, as no absolute cross sections were measured and the errors shown are the statistical standard deviations. The energies of the neutrons producing the events are shown in Table XXVI and Fig. 20. For comparison purposes the total corrected numbers of p-type and He-type events have been normalized to the total corrected number of d-type events. The errors are large (about ±8%) but the general trends are still indicative. In particular it might be noted that low-energy neutrons favor the He^3-type events as might be expected.

Because any theory comparing the results of this paper with the π^+ and π^o data[1, 5-7] requires an accurate energy spectrum, that given by DePangher[10] is included in Fig. 21.

No conclusions can be drawn from these results until the theoretical calculations are completed. At such a time a joint paper will be presented.

---

* If the neutron in the deuteron were directed exactly toward the incident neutron the cross section would be higher because of the steep excitation function, but the solid angle would be slightly larger for a neutron directed toward but at an angle to the incident neutron. Therefore the protons would be expected to be directed forward at small angles (0° to 30°) to the beam.

Table XXII

Pion Angular Distributions

Type of Event		Deuteron $n + d \rightarrow \pi^- + p + d$			Proton $n + d \rightarrow \pi^- + 2p + n$			He^3 $n + d \rightarrow \pi^- + He^3$		
θ	Ω^*	N	N_c	N_c/Ω	N	N_c	N_c/Ω	N	N_c	N_c/Ω
0 - 9.4	1.37	11	11.0	8.0 ± 2.4	1	1.0	0.7 ± 0.7	-	-	-
9.5 - 19.4	4.37	26	26.0	6.0 ± 1.2	12	12.0	2.8 ± 0.8	1	1.0	0.2 ± 0.2
19.5 - 29.4	7.22	36	36.0	5.0 ± 0.8	13	13.0	1.8 ± 0.5	6	6.0	0.8 ± 0.3
29.5 - 39.4	9.88	24	24.0	2.4 ± 0.5	9	9.0	0.9 ± 0.3	5	5.0	0.5 ± 0.2
39.5 - 49.4	12.22	25	25.0	2.0 ± 0.4	8	8.0	0.7 ± 0.2	4	4.0	0.3 ± 0.2
49.5 - 59.4	14.19	11	14.4	1.0 ± 0.3	9	11.6	0.8 ± 0.3	3	3.5	0.2 ± 0.1
59.5 - 69.4	15.73	11	17.1	1.1 ± 0.3	6	9.3	0.6 ± 0.3	2	3.0	0.2 ± 0.1
69.5 - 79.4	16.80	10	17.0	1.0 ± 0.3	5	8.5	0.5 ± 0.2	-	-	-
79.5 - 89.4	17.35	14	24.9	1.4 ± 0.4	3	5.3	0.3 ± 0.2	-	-	-
89.5 - 99.4	17.37	10	17.8	1.0 ± 0.3	3	5.4	0.3 ± 0.2	-	-	-
99.5 - 109.4	16.88	8	13.9	0.8 ± 0.3	1	1.7	0.1 ± 0.1	-	-	-
109.5 - 119.4	15.86	2	3.2	0.2 ± 0.1	2	3.0	0.2 ± 0.1	-	-	-
119.5 - 129.4	14.37	9	11.8	0.8 ± 0.3	2	2.4	0.2 ± 0.1	1	1.4	0.1 ± 0.1
129.5 - 139.4	12.43	4	4.0	0.3 ± 0.2	3	3.0	0.2 ± 0.1	-	-	-
139.5 - 149.4	10.12	5	5.0	0.5 ± 0.2	2	2.0	0.2 ± 0.1	-	-	-
149.5 - 159.4	7.51	1	1.0	0.1 ± 0.1	-	-	-	-	-	-
159.5 - 169.4	4.66	1	1.0	0.2 ± 0.2	-	-	-	-	-	-
169.5 - 180	1.67	-		-	1	1.0	0.6 ± 0.6	-	-	-

* $2\pi\Omega$ = 100 x the total solid angle in the θ interval.

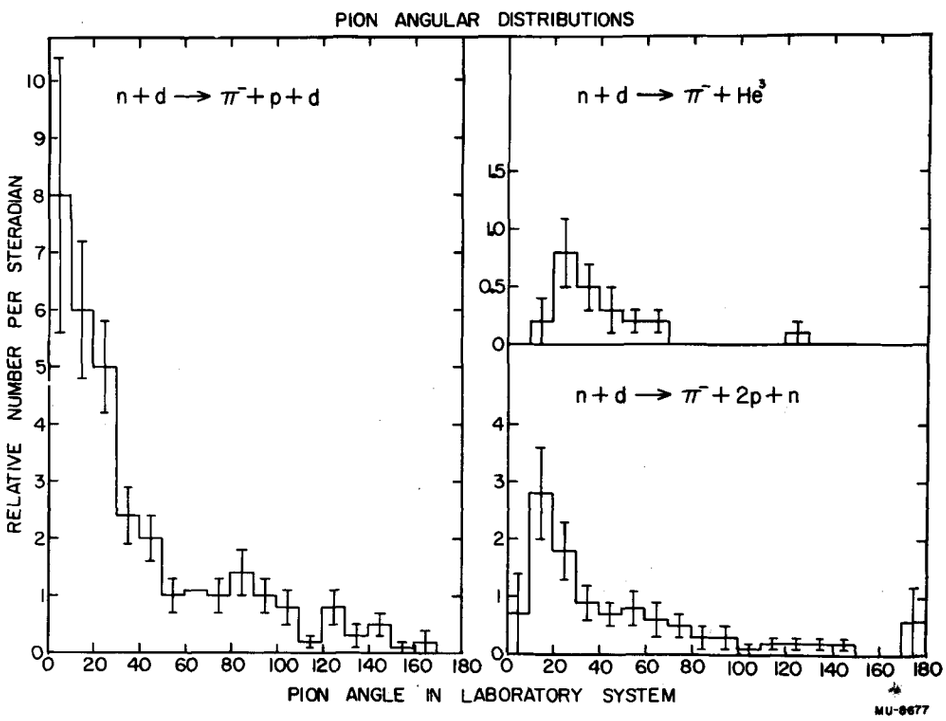

Figs. 14, 15 and 16 Pion laboratory-system angular distributions for the three reactions $n + d \rightarrow \pi^- + p + d$, $n + d \rightarrow \pi^- + 2p + n$, $n + d \rightarrow \pi^- + He^3$.

Table XXIII

Pion Energy Spectra

Type of Event	Deuteron $n + d \rightarrow \pi^- + p + d$		Proton $n + d \rightarrow \pi^- + 2p + n$		He^3 $n + d \rightarrow \pi^- + He^3$	
T_π(Mev)	N	N_c	N	N_c	N	N_c
0 - 9.4	27	38.5 ± 7.4	15	19.5 ± 5.0	-	-
9.5 - 19.4	37	49.8 ± 8.2	15	19.9 ± 5.1	1	1 ± 1
19.5 - 29.4	32	39.9 ± 7.1	14	16.4 ± 4.4	-	-
29.5 - 39.4	26	32.9 ± 6.5	16	19.1 ± 4.8	2	2.4 ± 1.7
39.5 - 49.4	20	23.0 ± 5.1	7	8.1 ± 3.1	1	1 ± 1
49.5 - 59.4	26	28.9 ± 5.7	3	3.4 ± 2.0	3	3.5 ± 2.0
59.5 - 69.4	16	16.0 ± 4.0	6	6.0 ± 2.5	6	6.5 ± 2.7
69.5 - 79.4	8	8.0 ± 2.8	2	2.0 ± 1.4	3	3.2 ± 1.8
79.5 - 89.4	6	6.0 ± 2.5	1	1.0 ± 1.0	2	2 ± 1.4
89.5 - 99.4	6	6.0 ± 2.5	1	1.0 ± 1.0	-	-
99.5 - 109.4	2	2.0 ± 1.4	-	-	2	2.1 ± 1.5
109.5 - 119.4	2	2.0 ± 1.4	-	-	1	1 ± 1
119.5 - 129.4	-	-	-	-	1	1.3 ± 1.3

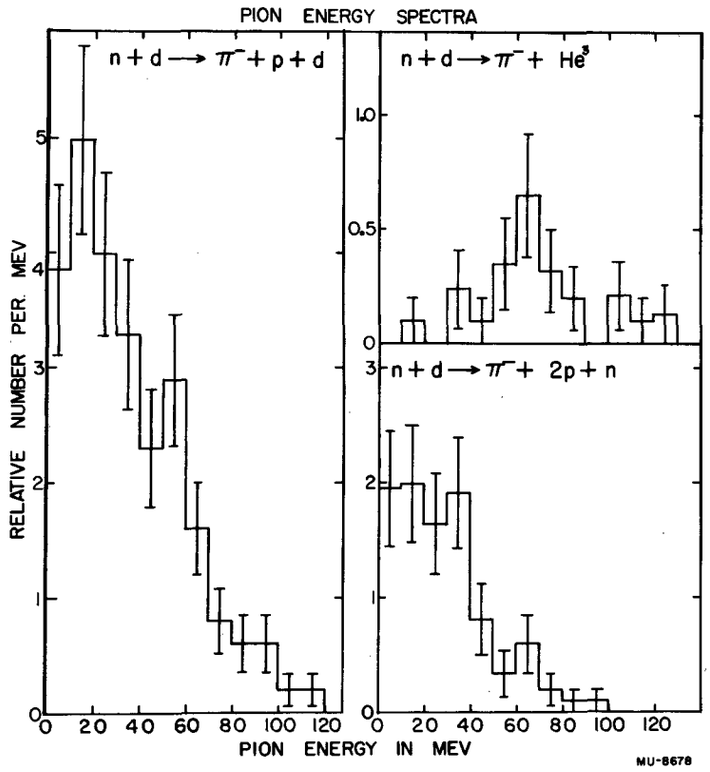

Figs. 17, 18, and 19 Pion laboratory-system energy spectra for the three reactions $n + d \rightarrow \pi^- + p + d$, $n + d \rightarrow \pi^- + 2p + n$, $n + d \rightarrow \pi^- + He^3$.

Table XXIV

Distributions for the Protons in $n + d \rightarrow \pi^- + p + d$

Angular Distribution

θ	Ω	N	N_c	N_c/Ω
.0 - 9.4	1.37	17	18.5	13.5 ± 3.3
9.5 - 19.4	4.37	32	34.5	7.9 ± 1.4
19.5 - 29.4	7.22	27	36.6	5.1 ± 1.0
29.5 - 39.4	9.88	33	42.1	4.3 ± 0.8
39.5 - 49.4	12.22	30	35.5	2.9 ± 0.5
49.5 - 59.4	14.19	18	22.9	1.6 ± 0.4
59.5 - 69.4	15.73	14	18.1	1.1 ± 0.3
69.5 - 79.4	16.80	6	6.8	0.5 ± 0.2
79.5 - 89.4	17.35	7	7.6	0.4 ± 0.2
89.5 - 99.4	17.37	4	4.8	0.3 ± 0.2
99.5 - 109.4	16.88	3	3.0	0.2 ± 0.1
109.5 - 119.4	15.86	2	2.8	0.2 ± 0.1
119.5 - 129.4	14.37	1	1.0	0.1 ± 0.1
129.5 - 139.4	12.43	0	0	0
139.5 - 149.4	10.12	0	0	0
149.5 - 159.4	7.51	0	0	0
159.5 - 169.4	4.66	0	0	0
169.5 - 180	1.67	0	0	0
Indeterminate*		14	16.0	

Energy Spectrum

T_π (Mev)	N	N_c
0 - 0.4	18	21.2
0.5 - 1.4	15	17.8
1.5 - 2.4	16	19.8
2.5 - 3.4	10	11.0
3.5 - 4.4	13	15.2
4.5 - 9.4	27	34.0
9.5 - 19.4	18	23.2
19.5 - 29.4	19	23.8
29.5 - 39.4	10	11.7
39.5 - 49.4	12	14.5
49.5 - 59.4	8	10.1
59.5 - 69.4	5	5.4
69.5 - 79.4	6	8.1
79.5 - 89.4	5	5.4
89.5 - 99.4	7	8.4
99.5 - 109.4	6	8.2
109.5 - 119.4	6	6.9
119.5 - 129.4	1	1.0
129.5 - 139.4	2	2.2
139.5 - 149.4	2	2.7
149.5 - 159.4	2	2.3

* The track is too short for its direction to be determined.

Table XXV

Relative Frequencies of the Three Reactions

Reaction	Number of Events of Each Type	Ratio of Each to the Total Number of Events
$n + d \rightarrow \pi^- + p + d$	208	67%
$n + d \rightarrow \pi^- + 2p + n$	80	26 %
$n + d \rightarrow \pi^- He^3$	22	7%
Total, All Reactions	310	

Table XXVI

Neutron Energy Spectra

	$n + d \rightarrow \pi^- + p + d$		$n + d \rightarrow \pi^- + 2p + n$		$n + d \rightarrow \pi^- + He^3$	
T_n(Mev)	N	N_c	N	$2.63\ N_c$	N	$10.5\ N_c$
220	-	-	-	-	1	10 ± 10
230	-	-	-	-	-	-
240	-	-	-	-	1	10 ± 10
250	1	1.0 ± 1.0	-	-	1	10 ± 10
260	2	2.8 ± 2.0	2	7 ± 5	2	21 ± 15
270	12	12.7 ± 3.7	-	-	3	32 ± 18
280	15	17.7 ± 4.6	2	6 ± 4	2	21 ± 15
290	20	24.3 ± 5.4	4	13 ± 6	4	49 ± 24
300	45	55.1 ± 8.2	11	30 ± 9	4	52 ± 26
310	37	47.2 ± 7.8	15	45 ± 12	-	-
320	40	47.5 ± 7.5	22	76 ± 16	1	10 ± 10
330	18	23.0 ± 5.4	11	37 ± 11	2	22 ± 16
340	18	21.8 ± 5.1	13	39 ± 11	1	13 ± 13

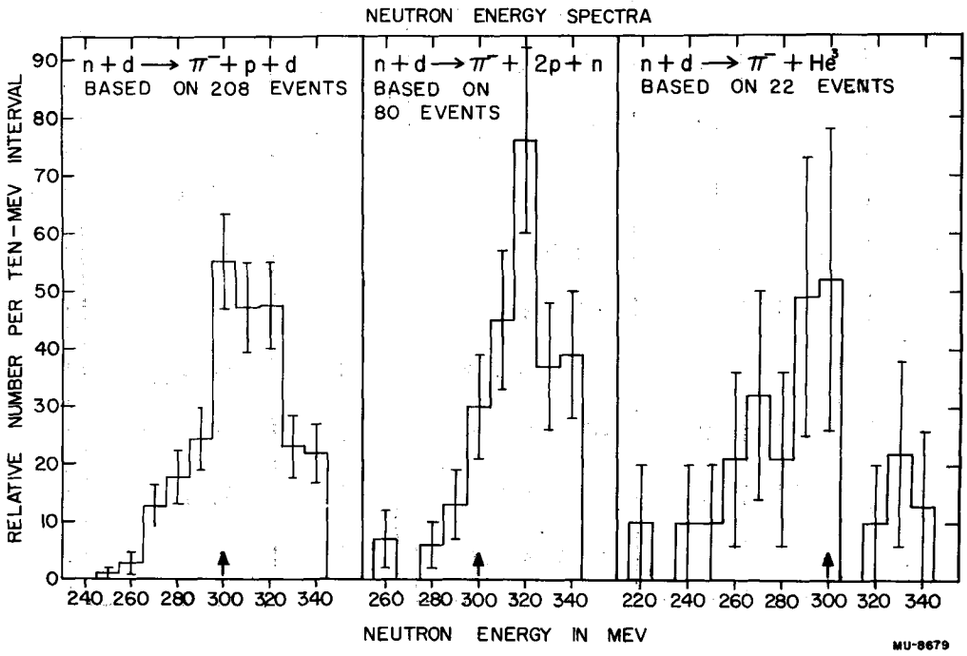

Fig. 20 Energy distributions of the neutrons that produce the events. The arrow at 300 Mev indicates the peak of the beam as obtained by De Pangher.

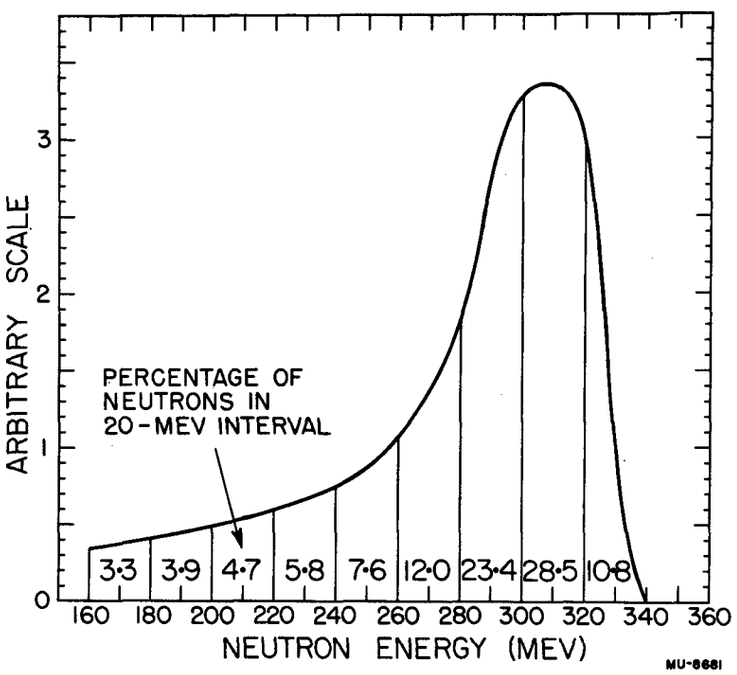

Fig. 21 Neutron energy spectrum as obtained by De Pangher

ACKNOWLEDGMENTS

To Professor Wilson M. Powell for suggesting this research topic, and for his guidance and encouragement throughout the course of the experiment, goes much of the credit for its success. Besides making available all of the facilities of the University of California Radiation Laboratory cloud chamber group, Professor Powell personally scanned a large portion of the film.

Acknowledgment cannot possibly be made to all persons who aided in the progress of this experiment, but their effort, even if unmentioned, deserves my deepest gratitude. Among those whose help made the cyclotron runs possible, supplying technical assistance as well as long hours of toil, were Messrs. John B. Elliott, Larry O. Oswald, Peter H. Moulthrop, George Saphir, Dr. Franklin C. Ford, and Dr. John DePangher, Jr. as well as many other present and past members of the cloud chamber group. The tedious job of measuring the remeasuring the tracks was accomplished with the help of many: notably Dr. Chung Ying Chih, Mr. John B. Elliott, and Mr. Harold Adelson. Most of the calculations were carried out by Mr. Howard S. White, Miss Barbara W. Schultz, Miss Nancy Peppin, and my wife, Dorris.

The designers of a few of the many pieces of equipment whose use either made the experiment possible or aided in its performance include the following: Professor Powell--the cloud chamber magnet; Dr. John DePangher--the cloud chamber and related equipment; Messrs. John Elliott and Larry Oswald--the automatic film developer attached directly to the camera; and Mr. Howard White--special slide rules for calculating θ and ϕ. Mr. White also introduced the author to the use of Keysort Cards.

APPENDICES

I. Range-Energy and Momentum-Energy Relations

In carrying out the calculations of this experiment the function scales shown in Figs. 22, 23, and 24 were found very useful. The magnetic rigidity of a particle was used directly as its momentum, and Figs. 22 and 23 enable one to get the energies of pions and protons respectively from these momentum units. As mentioned in the text, if both scales of Fig. 23 are multiplied by 2, deuteron energies are then given in terms of their magnetic rigidities. Figure 24 is the proton range-energy relation as derived from the curve of Aron et al.[17] Figures 23 and 24 were prepared by DePangher.[10]

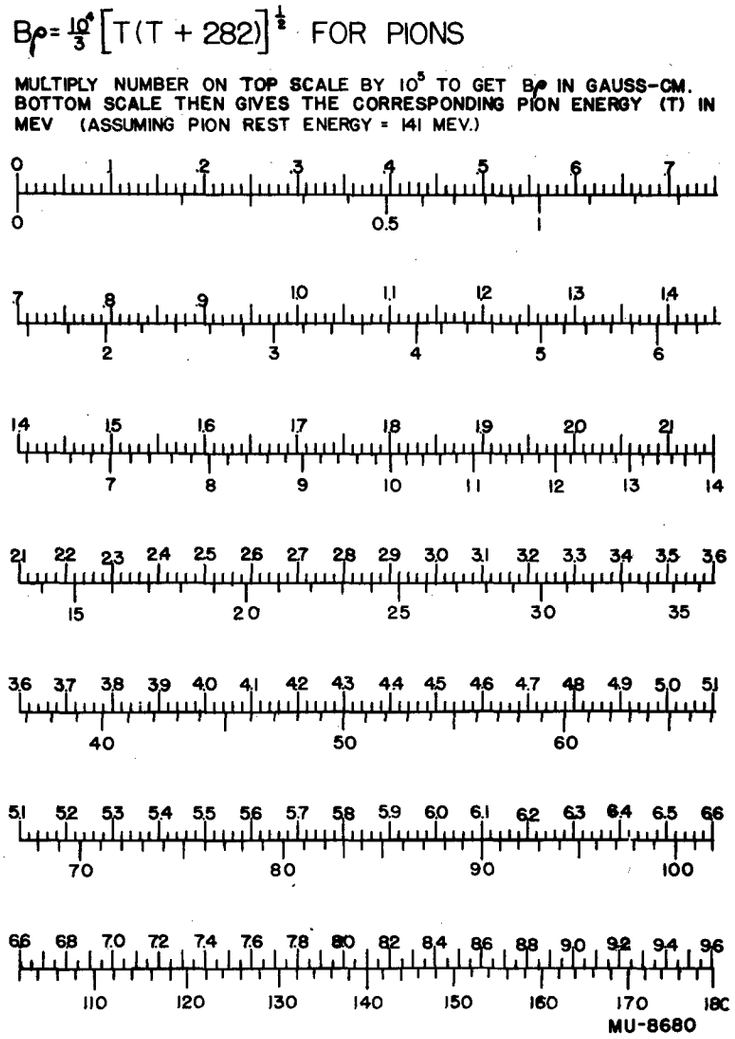

Fig. 22 Function scale giving Bρ vs kinetic energy for protons.

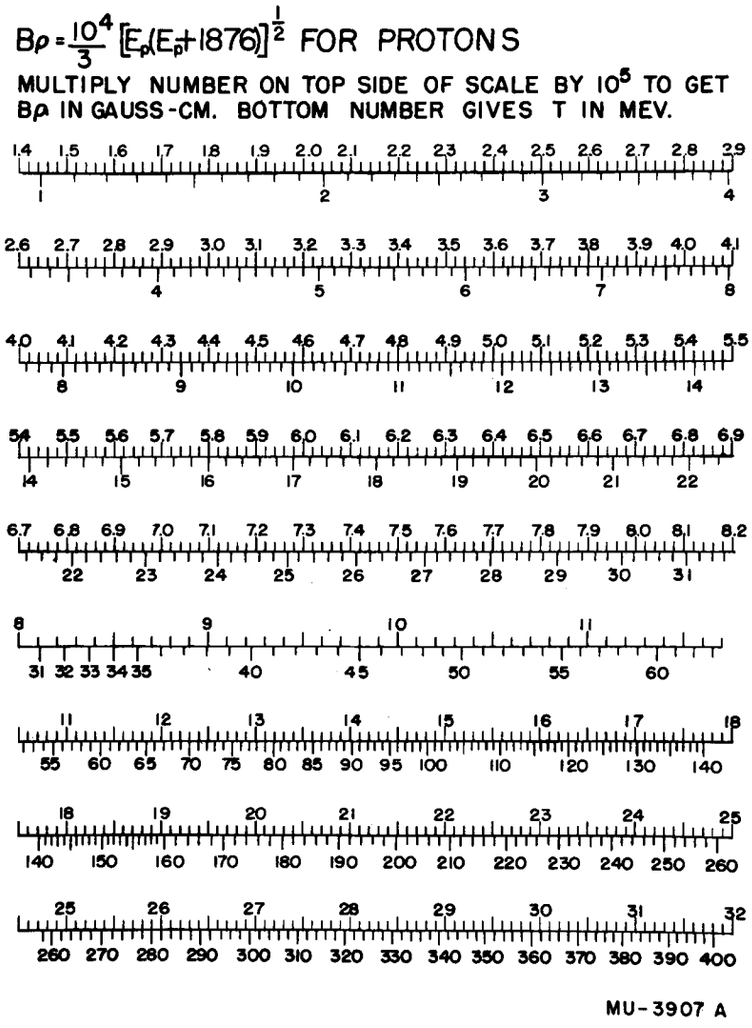

Fig. 23 Function scale giving Bρ vs kinetic energy for pions.

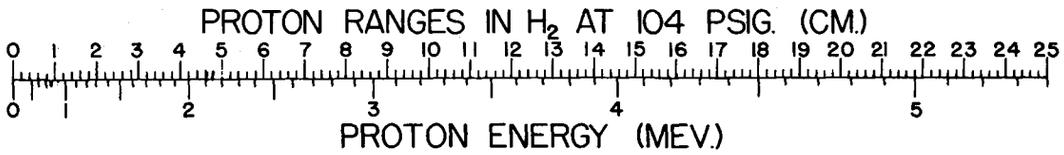

MU-8696

Fig. 24 Function scale giving proton ranges in the 10-atmosphere cloud chamber vs. proton energies.

BIBLOIOGRAPHY

1. Roger H. Hildebrand, Phys. Rev. 89, 1090 (1953).

2. Wilson J. Frank, Kenneth C. Bandtell, Richard Madey, and Burton J. Moyer, Phys. Rev. 94, 1716 (1954).

3. Robert A Schluter, Phys. Rev. 95, 639 (1954).

4. A. H. Rosenfeld, Phys. Rev. 96, 139 (1954)

5. W. F. Cartwright, C. Richman, M. N. Whitehead, and H. A. Wilcox, Phys. Rev. 91, 677 (1953)

6. Frank Stevens Crawford, Jr., "Reaction $p + p \rightarrow \pi^+ + d$", University of California Radiation Laboratory Report No. UCRL-2187, April, 1953.

7. M. Lynn Stevenson, "The Angular Distribution of the Reaction $p + p \rightarrow d \pi^+$ at 338 Mev", University of California Radiation Laboratory Report No. UCRL-2188, April, 1953.

8. A. M. L. Messiah, Phys. Rev. 86, 430 (1952).

9. M. Ruderman, Phys. Rev. 87, 383 (1952).

10. John DePangher, Jr , Phys. Rev. 95, 578 (1954). Also "A High-Pressure Cloud Chamber Investigation of Protons Scattered by 300-Mev Neutrons", University of California Radiation Laboratory Report No. UCRL-2153, March, 1953.

11. Peter E. Tannenwald, "Disintegration of Helium by 90-Mev Neutrons", University of California Radiation Laboratory Report No. UCRL-1767, April, 1952.

12. Franklin C. Ford, "The Production of Charged Pi Mesons by Neutrons on Oxygen" University of California Radiation Laboratory Report No. UCRL-2148, March, 1953.

13. Chung Ying Chih, "A Cloud-Chamber Study of the Scattering Cross Section of Protons by 90-Mev Neutrons at Extreme Angles", University of California Radiation Laboratory Report No. UCRL-2575, May, 1954.

14. S. C. Wright and R. A. Schluter, Phys. Rev. 95, 639 (1954).

15. Burns MacDonald, private communication.

16. Alvin George Schulz, Jr., "The Excitation Function for π^+- Mesons Produced in Proton-Proton Collisions at 0^o to the Beam", University of California Radiation Laboratory Report No. UCRL-1756, May 22, 1952.

17. W. A. Aron, B. G. Hoffman, and F. C. Williams, "Range-Energy Curves", University of California Radiation Laboratory Report No. UCRL-121, 1949.